EPJ Web of Conferences **6**, 20011 (2010)
DOI:10.1051/epjconf/20100620011

Free edge effects study in laminated composites using Digital Image Correlation: effect of material and geometrical singularities

P. Lecomte-Grosbras[1], B. Paluch[2], M. Brieu[1]

[1]EC-Lille, LML, Boulevard Paul Langevin, Cité Scientifique, 59655 Villeneuve d'Ascq France
[2]ONERA-Lille, DADS-CRD, 5 boulevard Paul Painlevé 59045 Lille Cedex France

Abstract. Composite materials are today used for various industrial applications. However, delamination on free edges, where stress gradients are strong, still remain a problem. In the aim of a better understanding of such phenomenons, Digital Image Correlation (DIC) measurements have been carried out on $[(15_n/-15_n)_2]_s$ laminates under uniaxial tensile strain. Three different composites with different mechanical properties and microstructure have been tested as well as two samples geometries: flat and with ply drop. Experimental results show high shear strain concentrations near 15°/-15° interlaminar interfaces on free edges which depend on material mechanical properties and microstructure and increase in the vicinity of a geometrical singularity.

1 Context and objectives

The use of composite materials has become more and more widespread in many industrial applications. Thanks to the Classical Laminates Theory (CLT), design of composite structures is today globally well mastered. However, local effects, such as delamination near free edges or junctions, still remain a problem. It has long been known that the difference between elastic properties of adjacent plies induces strong three-dimensional interlaminar stresses on laminate free edges, which could initiate delamination [1]. This stress state cannot be predicted by CLT and some stacking sequences can be more critical than others [2]. Thus, a better understanding of free edge effects is still required for the design of laminated structures.

During recent decades, numerous authors have studied this phenomenon following the precursor works of [3]. Thanks to the recent developments of full field measurement techniques, more detailed studies, at mesoscopic scales, can be carried out. In this context the aim of this work was to measure, by Digital Image Correlation (DIC), the displacement and strain fields on free edge of laminated composites in order to highlight the strain gradients at mesoscopic scale near interlaminar interfaces. Composites with carbon fiber and epoxy matrix with a $[(15_n/-15_n)_2]_s$ stacking sequence have been tested under uniaxial tensile loading. These composites have different microstructures and elastic properties to highlight the influence of such characteristics on free edge strain concentrations. Two different samples geometries have been tested: flat samples to study free edge effects only, and with ply drops to show the influence of a geometrical discontinuity on free edge effects.

2 Investigated materials and samples geometry

2.1 Microscopic observations

For two of the three studied composite materials, fibre arrangement inside each layer is almost "regular", with quite rectilinear interfaces (dashed lines on Fig. 1a). This microstructure will be called "pure unidirectional" (pure-UD) in comparison to the third one for which a much more heterogeneous repartition of the fibres, due to an alternation of areas with high fibre or resin contents, has been noticed. As it can be seen in Fig. 1b, the interfaces are no longer rectilinear and present a kind of waviness induced by the presence of weft yarns in the plies which interlace the fibre strands. These yarns prevent the fibres from spreading homogeneously after compaction during the curing cycle. Thereafter, this material microstructure will be referred as ''quasi-unidirectional" (quasi-UD).

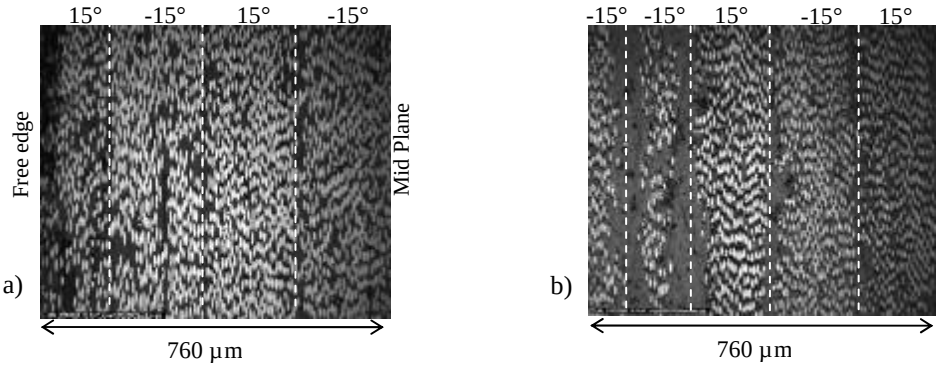

Fig. 1. Micrographic views of $[(15/-15)_2]_s$ laminates with "pure" (a) and "quasi" (b) UD microstructure

2.1 Macroscopic elastic properties

In addition to the previous described microstructures ("Pure-UD" and "Quasi-UD"), two types of carbon fibre (High Strength (HS) and High Modulus (HM)) have been used. It leads to three different composites, which properties are summarized in table 1. The elastic properties have been measured from tensile and shear tests, and their average values are given in table 1.

One may notice that the elastic properties of pure and quasi-UD-HS are similar, such that comparison between the results obtained on these two composite materials will highlight the microstructure influence on edge effects. The pure-UD-HS and HM samples have the same type of microstructure but elastic properties, mainly due to the fibre properties, are highly different. Thus, the comparison between the results obtained on these two materials will highlight the influence of mechanical properties on edge effects.

Table 1. Materials elastic properties

Designation	Material (supplier references)	E_1 (GPa)	E_2 (GPa)	G_{12} (GPa)	ν_{12}	Ply thickness h^0 (mm)
Pure-UD-HS	CTS/920	112	9	4	0.30	0.20
Quasi-UD-HS	G947/M18	116	8	3	0.30	0.18
Pure-UD-HM	M55J/M18	310	6	5	0.35	0.10

2.2 Samples stacking sequence and geometry

Two samples geometries have been considered: flat samples (Fig. 2a) to highlight edge effects only and samples with ply drops as shown in Fig. 2b.

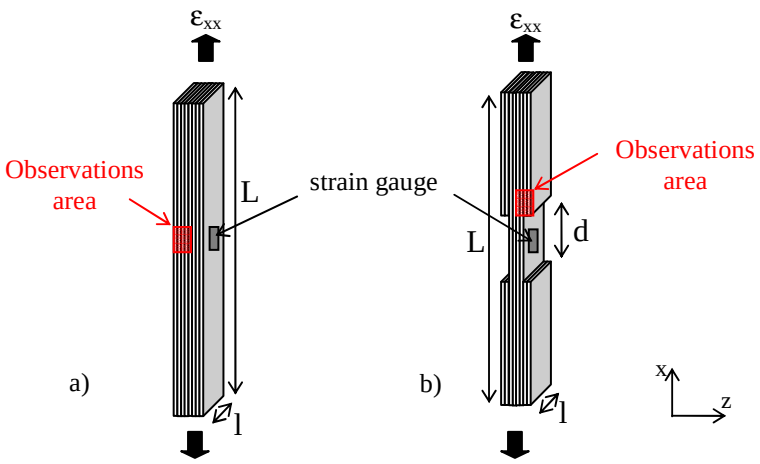

L (mm)	100
l (mm)	10
d (mm)	30

Fig. 2. Flat sample (a) sample with ply drops (b)

Flat samples have been manufactured with a $[(15_n/\text{-}15_n)_2]_s$ stacking sequence as edge effects, due to mismatches of elastic properties, are the most important and measurable for such orientations [3]. For results comparison, the layer thickness has to be the same in the three laminates. Since pure-UD-HM has a ply thickness about two times smaller than the other prepregs (see table. 1), $n = 1$ in pure-UD-HS and quasi-UD-HS samples and $n = 2$ in pure-UD-HM samples.

Samples with ply drops have been manufactured with pure-UD-HM composite with the two different stacking sequences $[0]_{16}$ and $[(15_2/\text{-}15_2)_2]_s$. The first one will show the influence of the geometrical singularity only, while the second one (where the ply drop is located at the 15°/-15° interlaminar interface) will show the influence of the staking sequence and ply drops on edge effects.

3 Experimental protocol and full field measurement technique

Fields measurements at mesoscopic scale using DIC technique with Aramis® software were carried out on samples free edge under uniaxial tensile loading.

3.1 Digital Image Correlation technique principle

The DIC technique consists in comparing two images of the same zone in the initial and deformed state. The initial image is divided into square facets of side length L, and spaced by the distance D (Fig. 3), each of them being characterized by its own grey level distribution. The principle is to find in the final image the most similar facet (in term of grey level distribution) in the reference image to calculate the local displacements in the centre of each facet. The strains in each facet are then calculated from the displacements in the adjacent facets using a centred finite difference algorithm.

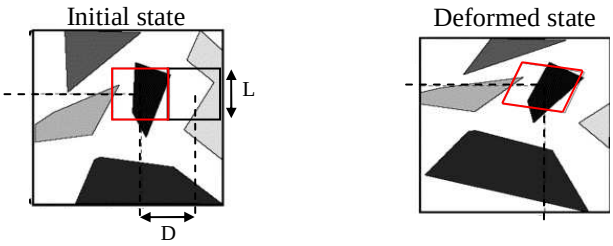

Fig. 3. DIC principle and definition of the (L,D) correlation parameters

Thus, to be analyzed by DIC, the observation area requires a random grey level distribution. Before the tests, samples edges had to be coarsely polished to observe the microstructure and obtain a random grey level distribution: light grey for fibres and dark grey for matrix as Fig. 1 reveals. In this way, the microstructure could be directly used to perform DIC treatments, without any paintings, as it is usually required.

Two different cameras have been used to capture the images on samples edge during tensile tests, with resolutions of 1024x1368 pixels and 2048x2736 pixels for the first and second one respectively. For DIC treatment, the (L,D) parameters have been set to (30, 20) pixels for pictures captured with the lowest resolution camera and to (60, 40) pixels for the second one. These parameters have been set to satisfy the best compromise between resolution and spatial resolution of DIC treatments [4]. The displacement and strain uncertainties have been estimated by applying a rigid body displacement of 20 µm of the sample fixed on a micrometric displacement table. The standard deviation on displacements and strains are smaller than 0.02 µm and 0.1 %.

3.2 Experimental protocol

The samples were loaded under uniaxial tensile strain with loading / unloading steps with increasing $<\varepsilon_{xx}>$ strain levels (the subscripts < > mean that ε_{xx} is the average strain on the overall sample). $<\varepsilon_{xx}>$ has been measured with a strain gauge fixed on the sample as shown on Fig. 2. At each strain level, a picture was captured on the samples edge and analyzed by DIC, by comparison with the first one taken at the initial undeformed state $<\varepsilon_{xx}> = 0$. Even pictures, subscript P_{2n}, correspond to a loaded state while the odd pictures, subscript P_{2n-1}, correspond to an unloaded state.

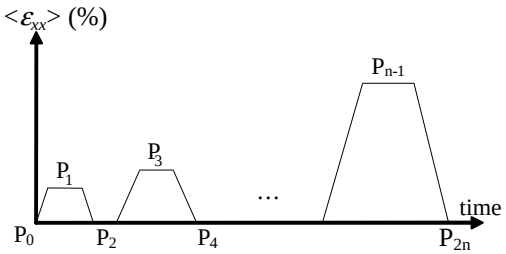

Fig. 3. Tensile test: loading / unloading steps

Image captures are carried out with an optical device, mounted on the frame of the tensile testing machine, consisting of a CCD Camera, a 12× zoom and a 10× long focal distance microscopic lens (Fig. 4) [5]. This optical device allows to observe areas from 0.2 to 2 mm width, with a focal distance of about 4 cm, such that the sample could easily be manipulated on the tensile testing machine. The device was fixed on three micrometric displacements tables to, on one hand, adjust the focal distance after each loading and unloading step and, on the other hand, to move the camera to reach the initial observation area which might move during the loading.

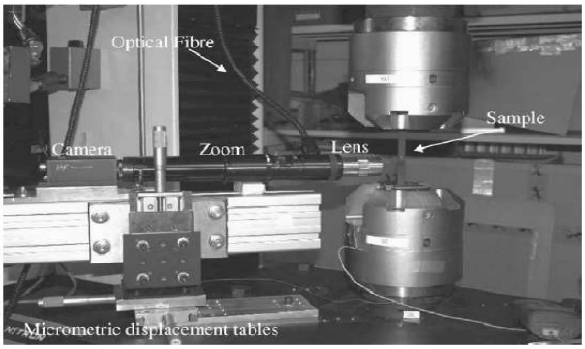

Fig. 4. Experimental set up

4 Experimental results

4.1 Edge effects in $[(15/-15)_2]_s$ pure-UD-HS laminates

Loading and unloading steps with increasing strain levels were applied to $[(15/-15)_2]_s$ pure-UD-HS laminates. At macroscopic scale the stress-strain relation is linear elastic until failure. Displacement and strain fields at mesoscopic scale have been measured on the free edge as illustrated on Fig. 2. The displacements u_x and shear strain fields ε_{xz} at a loading strain $\langle\varepsilon_{xx}\rangle = 0.4\%$ are shown on Fig. 5. High displacement and strain gradients (up to 5%) are clearly noticeable in the vicinity of 15°/-15° interfaces.

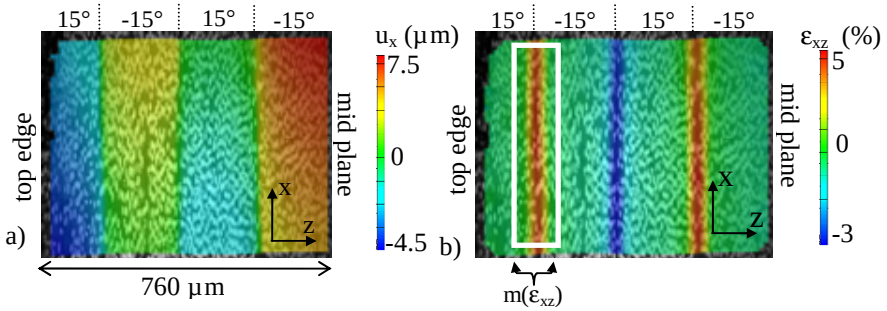

Fig. 5. u_x displacement (a) and ε_{xz} shear strain (b) measured on pure-UD-HS $[(15/-15)_2]_s$ laminate edge at $\langle\varepsilon_{xx}\rangle = 0.4\%$, DIC parameters (L,D) set to (30,20) pixels, 1 pixel = 0.55 µm

In order to study the variation of the shear strain ε_{xz} as a function of $\langle\varepsilon_{xx}\rangle$, the average value of ε_{xz} has been calculated along the first interface (white edge rectangle on Fig. 5b) and called $m(\varepsilon_{xz})$. On Fig. 6 the variation of $m(\varepsilon_{xz})$ has been plotted as a function of $\langle\varepsilon_{xx}\rangle$ in pure-UD-HS sample for loaded (plain line) and unloaded (dashed line) states and highlights a strong non-linear evolution of the averaged shear strains as well as residual shear strains appearance after unloading steps. These residual strains appear at early loading stages, and increase very quickly and non-linearly with $\langle\varepsilon_{xx}\rangle$.

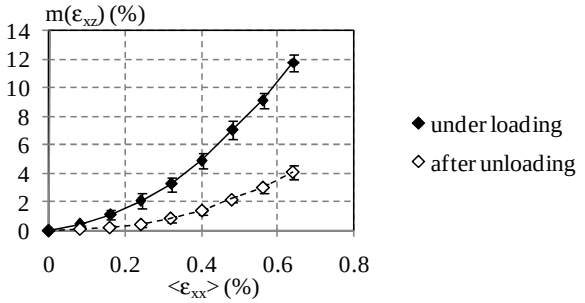

Fig. 6. Variation of $m(\varepsilon_{xz})$ at the first interface as a function of $\langle\varepsilon_{xx}\rangle$ in $[(15/-15)_2]_s$ pure-UD-HS samples

Images with higher magnification have also been taken at each loading and unloading steps to localize the origin of such residual strains. Fig 7, comparing images taken at unloaded state after applying different tensile strains $\langle\varepsilon_{xx}\rangle$, shows local damages which grow at ply interface.

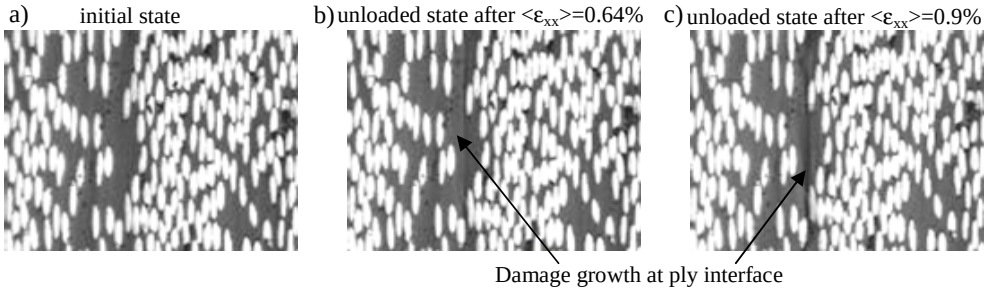

Fig. 7. Observation near 15°/-15° interface at microscopic scale in initial state and after $\langle\varepsilon_{xx}\rangle$=0.64% and 0.9% in $[(15/-15)_2]_s$ pure-UD-HS samples

The previous observations have been completed by SEM (Scanning Electron Microscope) inspections near the 15°/-15° interface and show more clearly than optical microscopy, the cracks at fibre/matrix interfaces and along the interlaminar interface (Fig. 8).

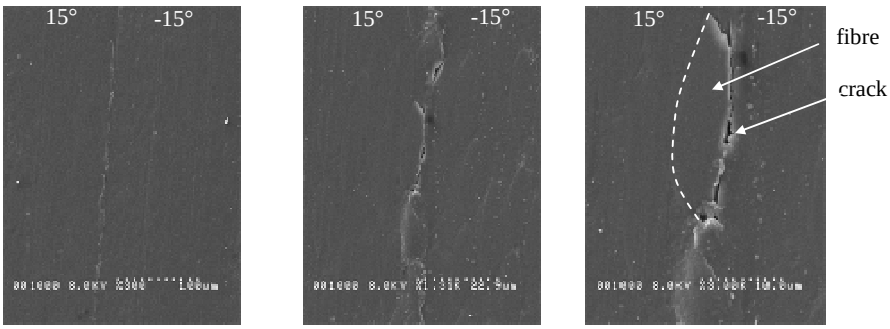

Fig. 8. SEM observations of damage at interlaminar interface in $[(15/-15)_2]_s$ pure-UD-HS samples

4.2 Influence of material mechanical properties and microstructure

The same tests were carried on pure-UD-HM $[(15_2/-15_2)_2]_s$ laminates where DIC results show the same trends, but with higher shear strain concentrations than in pure-UD-HS ones. In both laminates, $m(\varepsilon_{xz})$ varies non linearly as a function of $\langle\varepsilon_{xx}\rangle$ (Fig. 9). One can also notice that for the same $\langle\varepsilon_{xx}\rangle$ level, the magnitude of $m(\varepsilon_{xz})$ is higher in pure-UD-HM than in pure-UD-HS laminates, mainly due to the elastic properties of HM fibres.

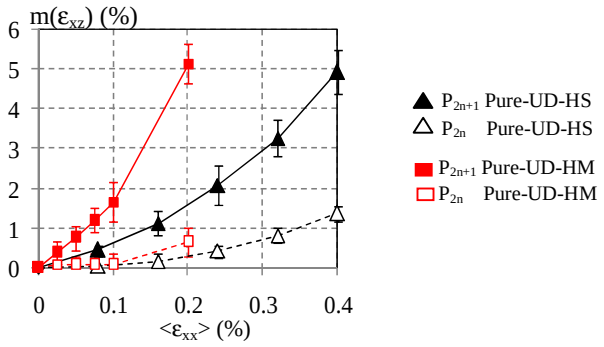

Fig. 9. Variation of $m(\varepsilon_{xz})$ at the first interface as a function of the macroscopic applied strain $<\varepsilon_{xx}>$ in pure-UD-HS and pure-UD-HM samples

In the same way, DIC measurements were carried out on quasi-UD-HS laminate edges (Fig. 10a the 15°/-15° interfaces are named I_1, I_2 and I_3). In this laminate, the inter-layer matrix thickness varies along each interface as well as the magnitude of ε_{xz} (Fig. 10b). The magnitude variation of ε_{xz} at I_1 and I_3 highlights that the thinner the interlaminar interfaces, the higher the shear strain concentrations.

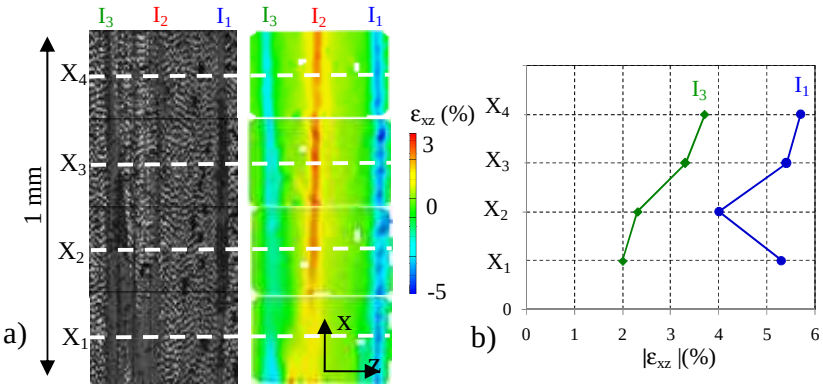

Fig. 10. a) ε_{xz} shear strain field on $[(15/-15)_2]_s$ quasi-UD-HS sample under $<\varepsilon_{xx}>=0.4\%$ with (L,D) = (30,20) and 1 pixel = 0.33 µm. b) Variations of ε_{xz} at I_1 and I_3 interlaminar interfaces along the free edge.

4.3 Influence of a geometrical discontinuity

DIC measurements on samples with dropped plies have been performed as illustrated on Fig. 11. For the $[0]_{16}$ stacking sequence there is no ply angle change and the shear strain concentration is only located in the vicinity of the dropped plies zone due to the geometrical singularity (Fig. 11a). For the second $[(15_2/-15_2)_2]_s$ stacking sequence, Fig. 11b shows shear strain concentrations along interlaminar interfaces which increase in the vicinity of the dropped plies zone (Fig 11c).

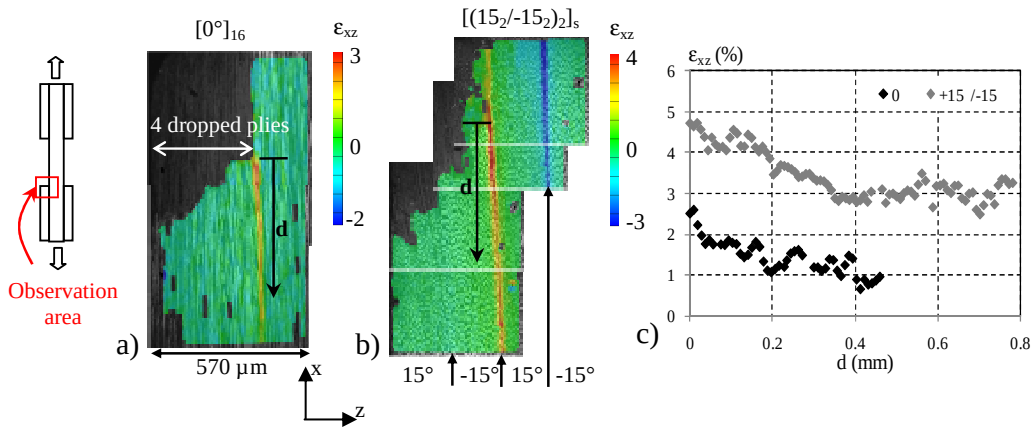

Fig. 11. ε_{xz} shear strain field in the vicinity of a ply drop with (L,D)=(60,40) and 1pixel = 0.21µm on [0]16 (a), and on $[(15_2/-15_2)_2]_s$ (b) pure-UD-HM free edge. c) Variation of ε_{xz} as function of the distance d to the ply drop.

5 Conclusions

The aim was to measure free edge effects in $[(15_n/-15_n)_2]_s$ laminates under uniaxial tensile loading using Digital Image Correlation Technique. For this purpose, an experimental procedure has been defined to use DIC at mesoscopic scale, such that no specific sample preparation is required, except a coarse polishing of the inspected area. Estimated uncertainties on displacements and strains, which are smaller than 0.02µm and 0.1% respectively, allow highlighting free edge effects with good accuracy. Very high shear strain concentrations have been measured in the vicinity of 15°/-15° ply interfaces, varying non-linearly as a function of the tensile strain, as well as residual shear strains after unloading. These residual strains increase have been linked to local damage growth at ply interface with SEM observations. Three different composite materials have been investigated to estimate the influence of elastic properties and microstructure on edge effect. Strain concentrations in pure-UD-HM samples are higher than in pure-UD-HS ones. In the same way, measurements on quasi-UD-HS samples show that edge effects are strongly depending on the local microstructure, and that shear strain concentrations decrease in high volume resin content areas. Finally, tensile tests on samples with dropped plies clearly show the influence of geometrical singularity on shear strain concentrations amplification.

Acknowledgements

The authors are grateful to the ‘‘Nord-Pas-de-Calais region”, the CISIT, the European Union, and the French Ministries of Defence and Research for their financial support.

References

1. CT. Herakovich. *J. of Comp. Mat*. **15**, 339–348 (1981).
2. RB. Pipes, NJ. Pagano. *J. of Comp. Mat*. **4**, 538–548 (1970).
3. NJ. Pagano, RB. Pipes. *J. of Comp. Mat.*, **5**, 50–57 (1971).
4. P. Lecomte-Grosbras, B. Paluch, M. Brieu, G. de Saxcé, L. Sabatier, *comp. Part A.* **40**, 1911–1920 (2009).
5. A. El Bartali, V. Aubin, S. Degallaix, *Fat. Frat. Eng. Mat. and Struct*., **31**, 137-151 (2007).